5-2013

Numerical Analysis of Non-Fickian Diffusion with a General Source

Ganesh Tiwari
University of New Orleans

Numerical Analysis of Non-Fickian Diffusion with a General Source

An Honors Thesis

Presented to

the Department of Physics

of the University of New Orleans

In Partial Fulfillment

of the Requirements for the Degree of

Bachelor of Science, with University Honors

and Honors in Physics

by

Ganesh Tiwari

May 2013

Acknowledgments

I would like to thank my parents and family members for encouraging me to pursue further education in Physics. Also, I am grateful to my thesis advisor, Dr. Ashok Puri, without whom I would not have been able to culminate my undergraduate career with an Honors degree. His valuable suggestions and instructions have assisted me not only in accomplishing the titled research but also to be able to think logically and independently as a growing researcher. In addition, I would like to thank Dr. George Ioup and Dr. Abu Kabir Mostofa Sarwar for their valuable assistance.

Table of Contents

List of Figures

ABSTRACT

The inadequacy of Fick's law to incorporate causality can be overcome by replacing it with the Green–Naghdi type II (GNII) flux relation. Combining the GNII assumption and conservation of mass leads to

$$\rho_{tt} - c_\infty^2 \rho_{xx} = (S(\rho))_t, \tag{1}$$

where $\rho(x,t)$ is the density function, $S(\rho)$ is a source term and c_∞ is a positive constant which carries (SI) units of m/sec. A general source term given by

$$S(\rho) = \gamma \left(\frac{\rho^m}{\rho_s^{m-1}} - \frac{\rho^n}{\rho_s^{n-1}} \right) \qquad n > m \geq 0, \tag{2}$$

is proposed. Here, the constants γ and ρ_s are the rate coefficient and saturation density respectively. The travelling wave solutions and numerical analysis of four special cases of equation (2), namely: Pearl-Verhulst Growth law, Zel'dovich Law, Newmann Law and Stefan-Boltzmann Law are investigated. For both analysis, results are compared with the available literature and extended for other cases. The numerical analysis is carried out by imposing well-studied Initial Boundary Value Problem and implementing a built-in method in the software package *Mathematica 9*. For Pearl-Verhulst source type, the results are compared to those found in literature [1]. Confirming the validity of built-in method for Pearl-Verhulst law, the generic built-in method is extended to study the transient signal response for similar initial boundary value problems when the source terms are Zel'dovich law, Newmann law and Stefan-Boltzmann law.

I. INTRODUCTION

Diffusion is one of the several natural transport phenomena. There are two approaches to the notion of diffusion, namely:

a. Atomistic Approach: According to this point of view, diffusion is considered as the result of the random walk of the dispersing particles. Brownian theory of motion is based on this approach [2].

b. Phenomelogical Approach: This methodology begins with Fick's law which postulates that the flux goes from the regions of high concentrations to the regions of low concentrations. In 1855, Adolf Fick proposed a steady flow law that was based on the same mathematical formalism as Fourier's law for heat conduction or Ohm's law for electricity [2, 3]. Fick's law states that the mass flux $\mathbf{q}$ is proportional to the density gradient $\nabla \rho$, that is,

$$\mathbf{q} = -D \nabla \rho, \tag{1}$$

where D is the coefficient of diffusion.

1.1 Development of Diffuson Models

Fick's law can be used to model various biological, physical and reaction diffusion systems. The continuity (mass conservation) equation is given by

$$\rho_t + \nabla \cdot \mathbf{q} = S(\rho, \mathbf{r}, t). \tag{2}$$

Here, $S(\rho, \mathbf{r}, t)$ is the source that accounts for the processes of the production and annihilation [4]. The subscript "t" indicates the partial differentiation of $\rho(\mathbf{r}, t)$ with respect to time. Taking the divergence of equation (1) and comparing with equation (2), we obtain

$$\rho_t - D \nabla^2 \rho = S(\rho, \mathbf{r}, t), \tag{3}$$

which is the general reaction-diffusion (RD) equation of the parabolic form that gives rise to various diffusion phenomena depending upon the source $S(\rho, \mathbf{r}, t)$. For instance, Fisher (1937) [5] and Kolmogoroff *et. al.* (1937) [6] independently proposed a model for the propagation of a mutant gene in a population through random mating in one-dimension with the source given by Pearl-Verhulst growth law as

$$S(\rho) = \gamma\rho(1 - \frac{\rho}{\rho_s}). \tag{4}$$

Combining equations (3) and (4) in one-dimension results in

$$\rho_t - D\rho_{xx} = \gamma\rho(1 - \frac{\rho}{\rho_s}), \tag{5}$$

which is known as Fisher-KPP equation. This equation has diverse applications not only in biological processes but also in physical processes such as nuclear reactor theory, branching Brownian motion and flame propagation [1, 7].

1.2 Generalization of the Source

Before delving more into the details of equation (3), source is taken into consideration. The motivation to this research comes from the desire in developing a general source term that represents a broad class of diffusion models. Recently, Jordan [1] published an analytical study of equation (5) with an emphasis on shock and related kinematic wave phenomena with the source being Pearl-Verhulst growth law while Bargmann [8] independently conducted analytical study when the source term was Zel'dovich law [9] and Newman law [10, 11]. Mathematically, Zel'dovich law is written as

$$S(\rho) = \gamma\rho_s \left(\frac{\rho}{\rho_s}\right)^2 \left(1 - \frac{\rho}{\rho_s}\right) \tag{6}$$

whereas Newmann law is given as

$$S(\rho) = \gamma\rho \left(1 - \left(\frac{\rho}{\rho_s}\right)^2\right). \tag{7}$$

Both Jordan and Bargmann also emphasized that the surface wave analysis of non-linear hyperbolic wave equations give rise to shock waves [1, 8]. Nonetheless, the source terms are different in the sense that Pearl-Verhulst law is evident in biological and physical processes as discussed earlier; Zel'dovich law is the representation of an autocatalytic reaction and Newmann law proposed by Newell and Whitehead to explain Rayleigh-Benard convection was applied by Newell to study diffusion problems in population genetics and combustion [1, 7, 9, 10, 11]. Particularly, both Pearl-Verhulst and Zel'dovich laws were studied by Rosen in the propagation of pressure waves in a combustion field [12]. In addition, Stefan-Boltzmann law which is applicable to high heat flux processes [13, 14] is given by

$$S(\rho) = \varepsilon\sigma(\rho_s^4 - \rho^4), \qquad (0 < \varepsilon < 1), \tag{8}$$

where ε is the emissivity, σ is the Stefan-Boltzmann constant and ρ_s is the temperature of the surrounding. The physical significance of ρ changes depending upon the diffusion process under study. When applied to a gene mutation study, ρ represents the population density in Pearl-Verhulst growth law and Newmann law. On the other hand, ρ denotes the concentration density in Zel'dovich law for autocatalytic reactions and temperature in Stefan-Boltzmann law, respectively. These four laws mentioned above fall into the category of a general source term given as

$$S(\rho) = \gamma\left(\frac{\rho^m}{\rho_s^{m-1}} - \frac{\rho^n}{\rho_s^{n-1}}\right) \qquad n > m \geq 0. \tag{9}$$

This generalization of the source can be applied not only to categorize a class of diffusion models but also to study such models with a general case inquiry.

1.3 Replacing Fick's Law with GN-II Flux Law

Although Fick's law adequately describes many diffusion processes, it is not applicable in all situations. For instance, the parabolic nature of equation (1) implies that the initial concentration pulse will propagate with infinite speed and the diffusion will be felt instantaneously [8]. Maxwell (1867) defined this contradictory feature as a "paradox of heat conduction (diffusion)" [4]. Researchers in heat conduction theory felt that the main cause of this anomaly is the fact that, according to Fourier's law, changes in the temperature gradient are instantaneously reflected in the thermal flux [1, 4, 8]. Among the various formulations to replace the Fick's law, Maxwell- Catteneo (MC) law [15] is the most promising; it predicts that the diffusion results from the damped temperature waves that propagates with finite speed and also introduces a relaxation time in order to delay the flux [1, 4, 8]. Mathematically, it is written as,

$$q + \tau_0 q_t = -\nu \rho_x \tag{10}$$

By letting $\tau_0 \to \infty$ and assuming $\nu / \tau_0 \to const. \equiv c_\infty^2$, equation (10) reduces to

$$q_t = -c_\infty^2 \rho_x , \tag{11}$$

which is the constitutive assumption known as Green-Nagdhi type II [16] in thermal theories [4, 8]. When Fick's law is replaced with Green-Nagdhi type II, the continuity equation takes the one-dimensional form

$$\rho_{tt} - c_\infty^2 \rho_{xx} = (S(\rho))_t . \tag{12}$$

Substituting the general source in equation (12) from equation (9), we get

$$\rho_{tt} - c_\infty^2 \rho_{xx} = \gamma \left(\frac{\rho}{\rho_s} \right)^{m-1} \left(m - n \left(\frac{\rho}{\rho_s} \right)^{n-m} \right) \rho_t \cdot , \tag{13}$$

which is a class of strictly non-linear (for $m \neq n$) hyperbolic partial differential equation offering more realistic models to various biological, physical and chemical reaction based diffusion processes.

1.4. Organization of Thesis

Having derived the general equation (13) of interest, the next step will be to investigate the solutions arising from various cases of the general source. In Section 2, integral equation approach for deriving travelling wave solutions (TWS) and built-in method in *Mathematica* for transient wave analysis of a well-posed dimensionless initial boundary value problem (IBVP) are applied.

The analytical and numerical results for various source terms are presented in Section 3. Comparisons are drawn with existing literature whenever available. Finally, based on the coefficients of right hand side of equation (13), an attenuation analysis is performed followed by brief discussions and conclusions.

I.   METHODS OF INVESTIGATION

Equation (13) arises in a wide range of diffusion systems whose source is governed by equation (9). The main objective of this research is to investigate how the wave evolves for different values of m and n in the source term. This study is conducted by exploring the travelling wave and numerical analysis of four special cases, namely: Pearl-Verhulst growth law, Zeld'ovich law, Newmann law and Stefan-Boltzmann law. The results obtained from the analysis are compared with the literature and then extended to other cases.

2.1 Travelling Wave Analysis

From plasma physics to biology, the study of nonlinear waves offers more approximate models to study several phenomena [5, 6, 18]. Unlike linear wave theory, in which one can easily apply Fourier analysis to solve the TWS, nonlinear wave theory has to be dealt with a variety of approximate methods [18]. For travelling wave analysis, the inadequacy of a formal generalized method has attracted the attentions of scientists in the related field for the proposition of a common method [18, 19, 20]. This thesis focuses in devising a generalized equation from equation (13) so that TWS foe each case can be easily derived. Since equation (13) is invariant under the transformation $x \rightarrow - x$, it is assumed that

$$\rho(x,t) = f(\xi) , \tag{14}$$

where $\xi = \beta(x - \upsilon t)$ with β being a constant whereas υ, the wave (propagation) speed is a positive constant. Substituting this transformation into equation (13) and integrating once yields

$$\beta(\upsilon^2 - c_\infty^2)f' + \gamma\upsilon\left(\frac{f^m}{\rho_s^{m-1}} - \frac{f^n}{\rho_s^{n-1}}\right) = \kappa. \tag{15}$$

Here κ is the constant of integration and a prime denotes differentiation with respect to ξ.

Provided that the integral $\int \dfrac{df}{\kappa - \gamma\upsilon\left(\dfrac{f^m}{\rho_s^{m-1}} - \dfrac{f^n}{\rho_s^{n-1}}\right)}$ be determined, the TWS for any particular

case of a given value of m and n can be successively derived.

2.2 Numerical Analysis

The strictly hyperbolic nature of equation (13) has the potential of giving rise to shock waves. However, the shock wave analysis is limited within the shock wave region. To quantitatively study the evolution of waves beyond the shock region, computational tools and methods have to be employed. In order to conduct a successful numerical analysis, a well-studied IBVP [1] given by

$$
\begin{cases}
\rho_{tt} - c_\infty^2 \rho_{xx} = \gamma\left(\dfrac{\rho}{\rho_s}\right)^{m-1}\left(m - n\left(\dfrac{\rho}{\rho_s}\right)^{n-m}\right)\rho_t, & (x,t) \in (0,\ell) \times (-\infty, t_f); \\[4mm]
\rho(0,t) = \rho_c^+ - A_0[H(t) - H(t - t_f)]Sin\left(\pi\dfrac{t}{t_f}\right) \qquad \rho(\ell,\, t) = \rho_c^+, \quad t < t_f; \\[4mm]
\rho(x,0) = \rho_c^+, \qquad \rho_t(x,0) = 0, \qquad x \in (0,\ell);
\end{cases}
\qquad (16)
$$

is considered; here, $H(.)$ represents the Heaviside Unit Step function, the constant $A_0 \in (0, \rho_s]$

denotes the amplitude of the input ' pulse', $\rho_c^+ \in (0, \rho_s]$ and $t_f = \dfrac{\ell}{c_\infty}$ is the duration (or width) of

the pulse. Introducing the dimensionless variables,

$$
\bar{\rho} = \frac{\rho - \rho_c^+}{\rho_s}, \qquad \bar{x} = \frac{x}{\ell}, \qquad \bar{t} = \frac{t}{t_f}, \qquad (17)
$$

the IVBP is simplified into non-dimensional form

$$\begin{cases} \rho_{tt} - \rho_{xx} = \gamma^* \left(\rho + \alpha\right)^{m-1} \left(m - n\left(\rho + \alpha\right)^{n-m}\right)\rho_t, & (x,t) \in (0,1) \times (-\infty,1); \quad (18a) \\ \rho(0,t) = \varepsilon[H(t) - H(t-1)]Sin\left(\pi t\right) \qquad \rho(1,\ t)\ = 0, \quad t < 1; & (18b) \\ \rho(x,0) = 0, \quad \rho_t(x,0) = 0, \quad x \in (0,1); & (18c) \end{cases}$$

where the bars have been omitted but understood, $\alpha = \dfrac{\rho_c^+}{\rho_s}$, $\gamma^* = \gamma t_f$ and $\varepsilon = \dfrac{A_0}{\rho_s}$.

2.2.1 Generic Finite Difference Scheme

Whenever one attempts to perform numerical analysis of partial differential equations, method of finite differences is adopted [1]. Following the footstep of Jordan [1], the simple discretization of equation (18a) is considered:

$$\frac{\rho_h^{k+1} - 2\rho_h^k + \rho_h^{k-1}}{(\Delta x)^2} - \frac{\rho_{h+1}^k - 2\rho_h^k + \rho_{h-1}^k}{(\Delta t)^2} = \gamma^* \left(\rho_h^k + \alpha\right)^{m-1} \left(m - n\left(\rho_h^k + \alpha\right)^{n-m}\right)\left(\frac{\rho_h^{k+1} - \rho_h^{k-1}}{2(\Delta t)}\right), (19)$$

where $x_h = h\Delta x$, $t_k = k\Delta t$ and $\rho(x,t) \approx \rho(x_h,t_k)$. The explicit scheme for the most advanced time-approximation is given by

$$\rho_h^{k+1} = \frac{R^2 \rho_{h+1}^k - 2(1 - R^2)\rho_h^k - \left[\dfrac{k\gamma^*}{2}(\rho_h^k + \alpha)^{m-1}\{m - n(\rho_h^k + \alpha)^{n-m}\} + 1\right]\rho_h^{k-1} + R^2 \rho_{h-1}^k}{1 - \dfrac{k\gamma^*}{2}(\rho_h^k + \alpha)^{m-1}\{m - n(\rho_h^k + \alpha)^{n-m}\}}, \quad (20)$$

where $R = k/h$ and the truncation error is given by $O[h^2 + k^2]$. Implementing an algorithm for equation (20), one can easily analyze the transient response based on equation (18) by performing a case by case analysis as in literature [1]. Nevertheless, in order to implement an algorithm for equation (17), one has to consider the discretization of values of Δx, Δt and R

wisely. Even though one may be able to perform clear and informative analysis with the aid of an algorithm, the values chosen may be irrelevant to the desired phenomenon under study [1].

2.2.2 Built-in Finite Difference Method

In order to reduce the complexity in carrying out the numerical analysis of IVBP denoted by equations (18a), (18b) and (18c), built-in methods in *Mathematica* 9 are subscribed and interweaved in the simplest manner to apply "NDSolve". The built-in method used in solving the IVBP is *Method of Lines*.

Method of Lines allows us to discretize in spatial dimension. The PDEs must be well posed as an initial (Cauchy) value problem in at least one dimension in order for this method to be applied. Since spatial variables are the ones to which the discretization is done and temporal variable to be found, we use the default value "TensorProductGrid" in the "Spatial Discretization" option. The "TensorProductGrid" uses discretization methods for one spatial dimension and uses an outer tensor product to derive methods for multiple spatial dimensions on rectangular regions. The maximum value the difference order can take is determined by the number of points in the grid. A limiting order is commonly referred to as "Pseudospectral"; however, "Pseudospectral" has a drawback that artificial oscillations (Runge's phenomenon) can be extreme. To avoid such oscillations, "Pseudospectral" method is replaced with "Minpoints" and "PrecisionGoal" methods. While implementing the NDsolve for IBVP, a warning message about inconsistent boundary conditions is issued. This happens due to the discretization error in approximating the boundary conditions. The error occurs because the spatial error estimates used to determine how many points to discretize with are based on initial conditions and PDE not boundary condition [21].

3. RESULTS

In this section, TWS derived from equation (15) and transient signal response for IBVP from equation (18) for Pearl-Verhulst growth law, Zel'dovich law, Newmann law and Stefan-Boltzmann law are presented.

The sequences shown in figures I – XVI show the evolution of the normalized relative density profiles ρ/ε versus x different values of α, where x corresponds to the interval $x \in (0,\ 1)$. The choice of values of parameters was based on the need for comparison with the literature [1] and for clear, informative graphs. The values chosen may not necessarily correspond to a particular diffusion system. Moreover, attenuation analysis for each law is carried out, respectively.

3.1 Pearl-Verhulst Growth Law

For Pearl-Verhulst growth law, equation (15) takes the form

$$\beta(\upsilon^2 - c_\infty^2)f' + \gamma\upsilon\left(f - \frac{f^2}{\rho_s}\right) = \kappa. \tag{21}$$

Separating the variables and integrating once results in

$$\int \frac{df}{\kappa - \gamma\upsilon\left(f - \dfrac{f^2}{\rho_s}\right)} = \frac{\xi}{\beta(\upsilon^2 - c_\infty^2)} + \text{constant}$$

When solved in *Mathematica 9*, the integral on the left takes the form of ArcTanh and the equation reduces to

$$\frac{2\sqrt{\rho_s}\,ArcTanh\left[(\rho_s - 2f)\sqrt{\dfrac{\gamma\upsilon}{\rho_s(\rho_s\gamma\upsilon - 4\kappa)}}\right]}{\sqrt{\gamma\upsilon(\rho_s\gamma\upsilon - 4\kappa)}} = \frac{\xi}{\beta(\upsilon^2 - c_\infty^2)} + constant.$$

$$\text{Hence, } f(\xi) = \frac{\rho_s}{2} - \frac{\phi}{4\lambda}Tanh\left[\lambda\phi\left\{\frac{\xi}{\beta(\upsilon^2 - c_\infty^2)} + constant\right\}\right] \tag{22}$$

is the required TWS for Pearl-Verhulst growth law with $\phi = \sqrt{(\rho_s\gamma\upsilon - 4\kappa)}$ and $\lambda = \dfrac{1}{2}\sqrt{\dfrac{\gamma\upsilon}{\rho_s}}$. The

solution represented by equation (22) has similar form of Tanh as in literature [1] and the

solution in literature [1] is a special case of TWS given by equation (22). It should be noted that

Jordan [1] derived the TWS for this case using Riccati equation.

Figures I – IV show the time evolution of relative density profiles for Pearl-Verhulst growth law.
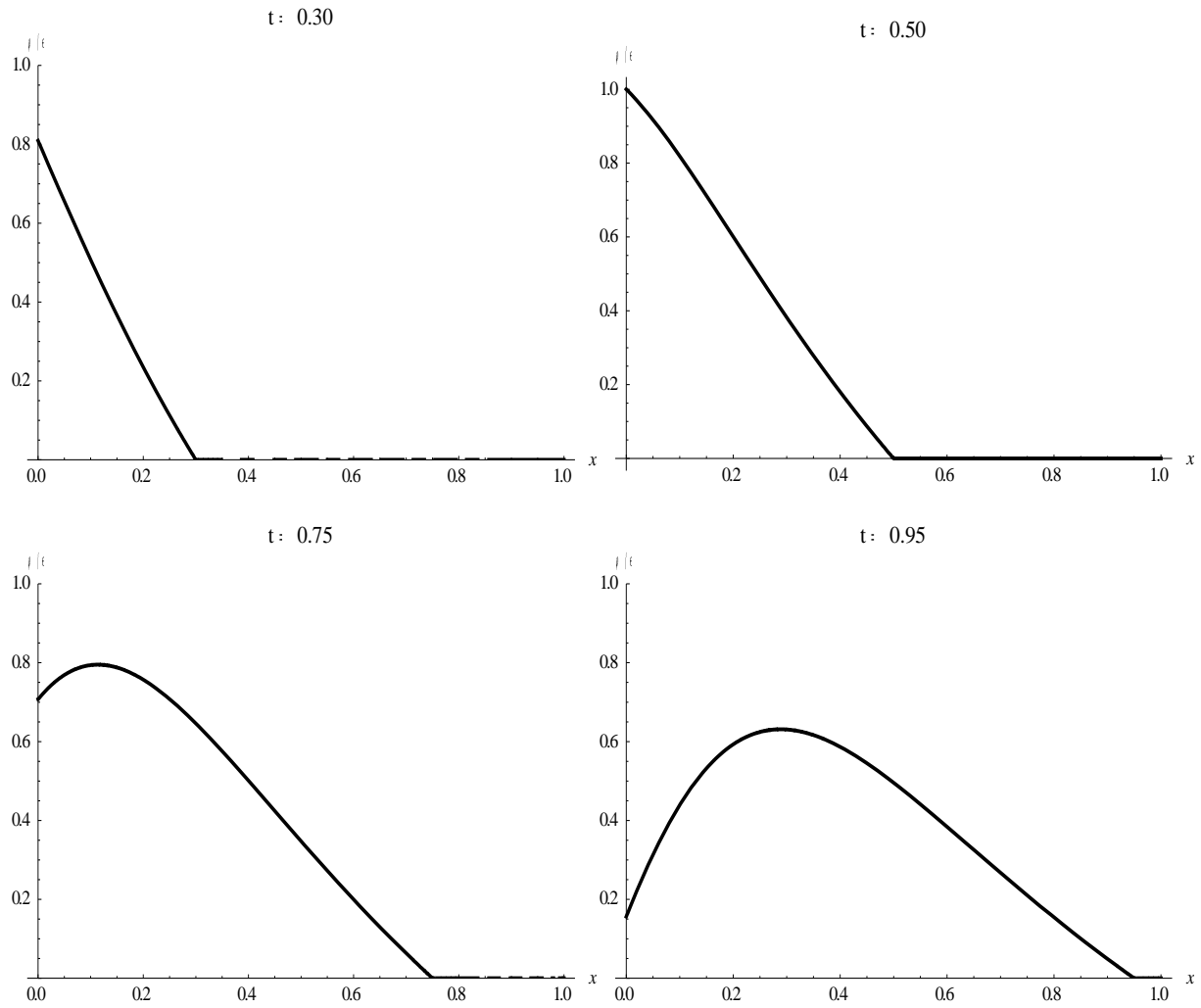
Fig. I: ρ/ε versus x for Pearl-Verhulst law for $\alpha = 0.75$, $\gamma^* = 5.0$ and $\varepsilon = 0.25$.
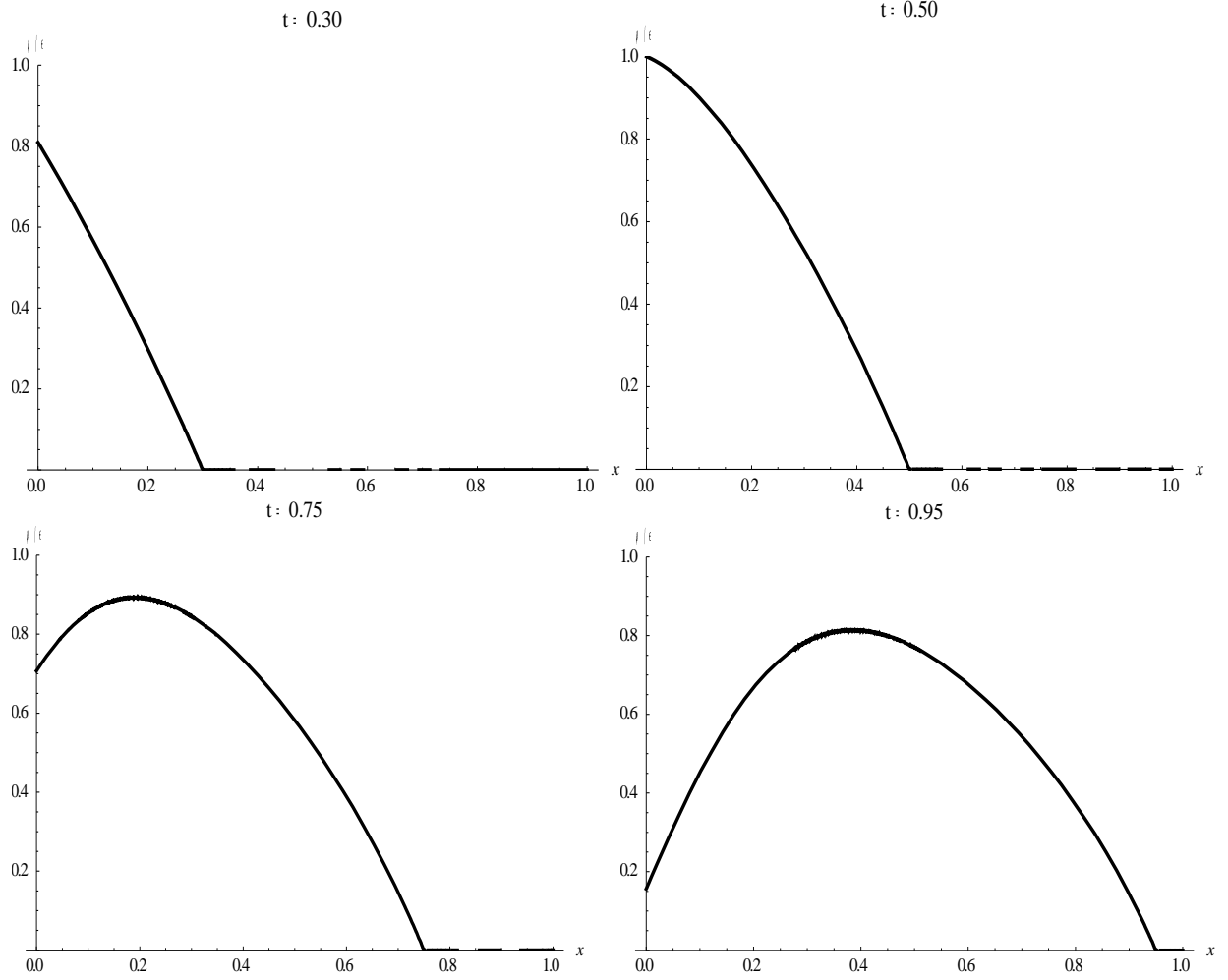
Fig. II: ρ/ε versus x for Pearl-Verhulst law for $\alpha = 0.50$, $\gamma^* = 5.0$ and $\varepsilon = 0.25$.
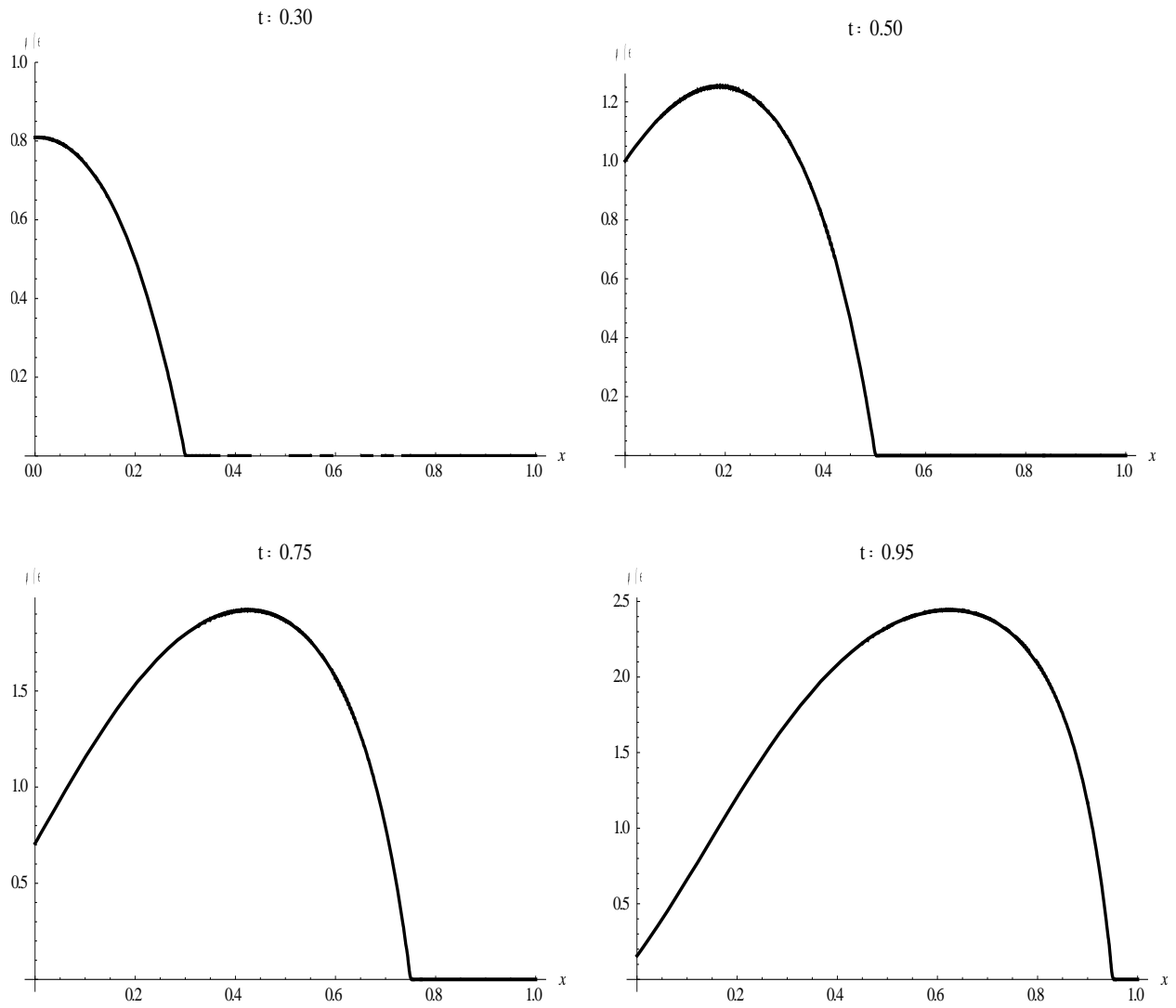
Fig. III: ρ/ε versus x for Pearl-Verhulst law for $\alpha = 0.0$, $\gamma^{*} = 5.0$ and $\varepsilon = 0.25$.

t: 0.30

t: 0.50

t: 0.75

t: 0.95
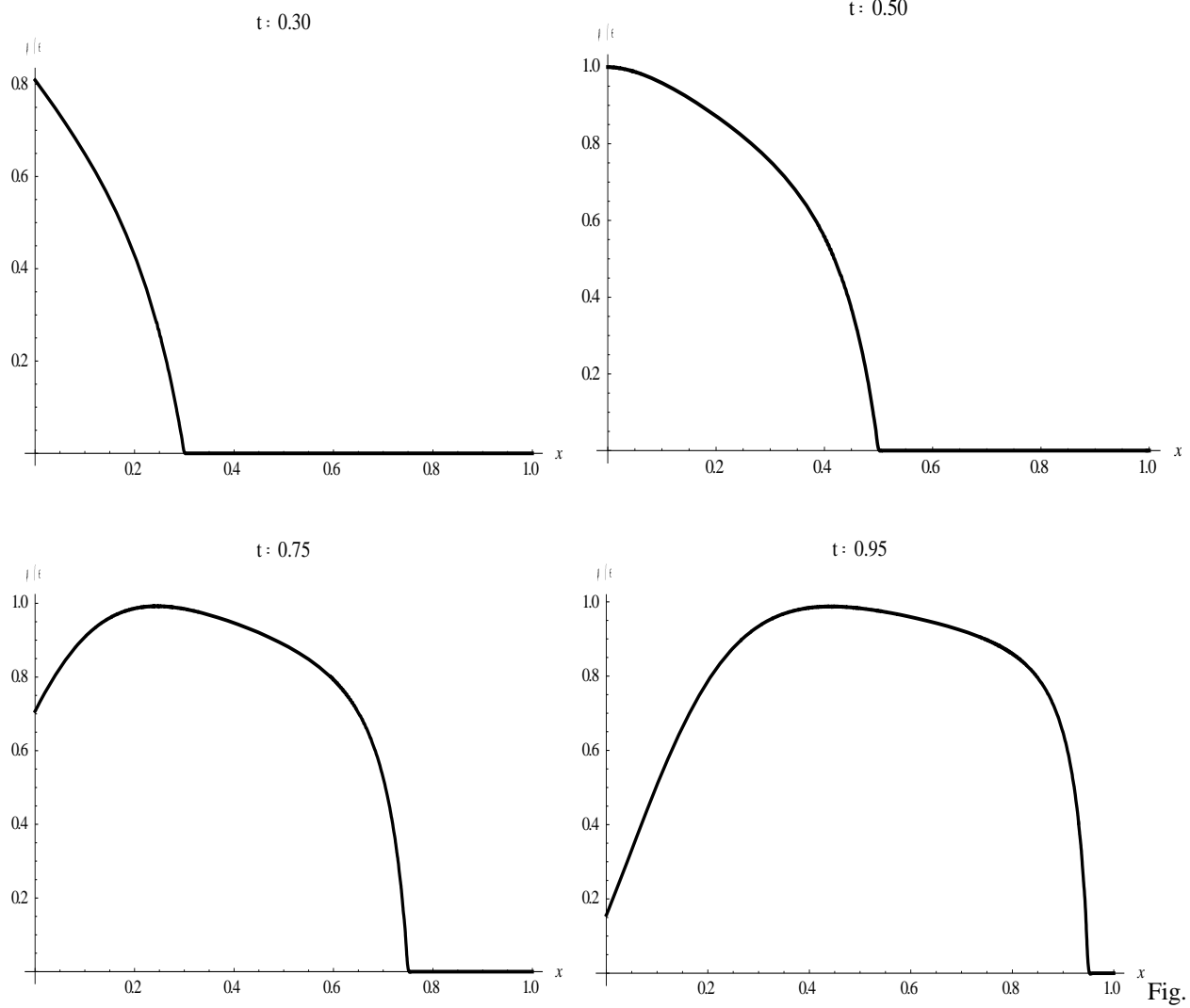
Fig. IV: ρ/ε versus x for Pearl-Verhulst law for $\alpha = 0.0$, $\gamma^* = 5.0$ and $\varepsilon = 1.0$.

In Fig. I and Fig. II, both profiles suffer attenuation. Since these profiles were generated for $\alpha = 0.75$ and $\alpha = 0.50$ respectively, the profiles behave as expected based on the fact that the coefficient of the term ρ_t is strictly negative for $\alpha \geq 0.5$ as mentioned [1] . Further analysis of Fig. I and II were carried out in terms of singular surface theory and acceleration wave in literature [1]. However, our attention is restricted only to confirm our scheme for carrying out the numerical simulation and performing the attenuation analysis based on the coefficient of ρ_t in equation (18a). Unlike figures I and II, the density profile suffer amplification for $\alpha = 0.0$ as shown in Fig. III; by t = 0.5, the peak value of ρ/ε already exceeds the input impulse [1]. From the last profile of Fig. III, it is clear that peak value of ρ/ε even exceeds 0.5. If $\rho < 0.5$, the coefficient of ρ_t would have been positive and negative for $\rho > 0.5$. In the literature [1], the seemingly conflicting effect of amplification observed in figure III was found to be in agreement with the analysis of singular surface theory. The profiles observed in Fig. IV for $\alpha = 0.0$ and $\varepsilon = 1.0$ also resemble those of literature [1]. Similar analysis is carried out for other source terms, respectively.

3.2 Zel'dovich Law

Repeating the integral approach with Zel'dovich law, the value of $\displaystyle\int \frac{df}{\kappa - \gamma\upsilon\left(\dfrac{f^2}{\rho_s} - \dfrac{f^3}{\rho_s^2}\right)}$ is

calculated using *Mathematica 9*. The obtained value being a root sum of slot functions is not suited for performing travelling wave analysis. However, for $\kappa = 0$, the integral reduces to a sum of reciprocal of f and natural logarithmic functions of f and the implicit TWS given by

$$\frac{\rho_s}{f} + \ln\left[\frac{f - \rho_s}{f}\right] = \gamma\upsilon\left(\frac{\xi}{\beta(\upsilon^2 - c_\infty^2)} + \text{constant}\right),$$

is obtained. This is in agreement with the literature [8]. Bargmann [8] even found the explicit TWS for a special case in terms of Lambert W function.

The figures V – VIII represent the time evolution of relative density profiles for Zel'dovich law.
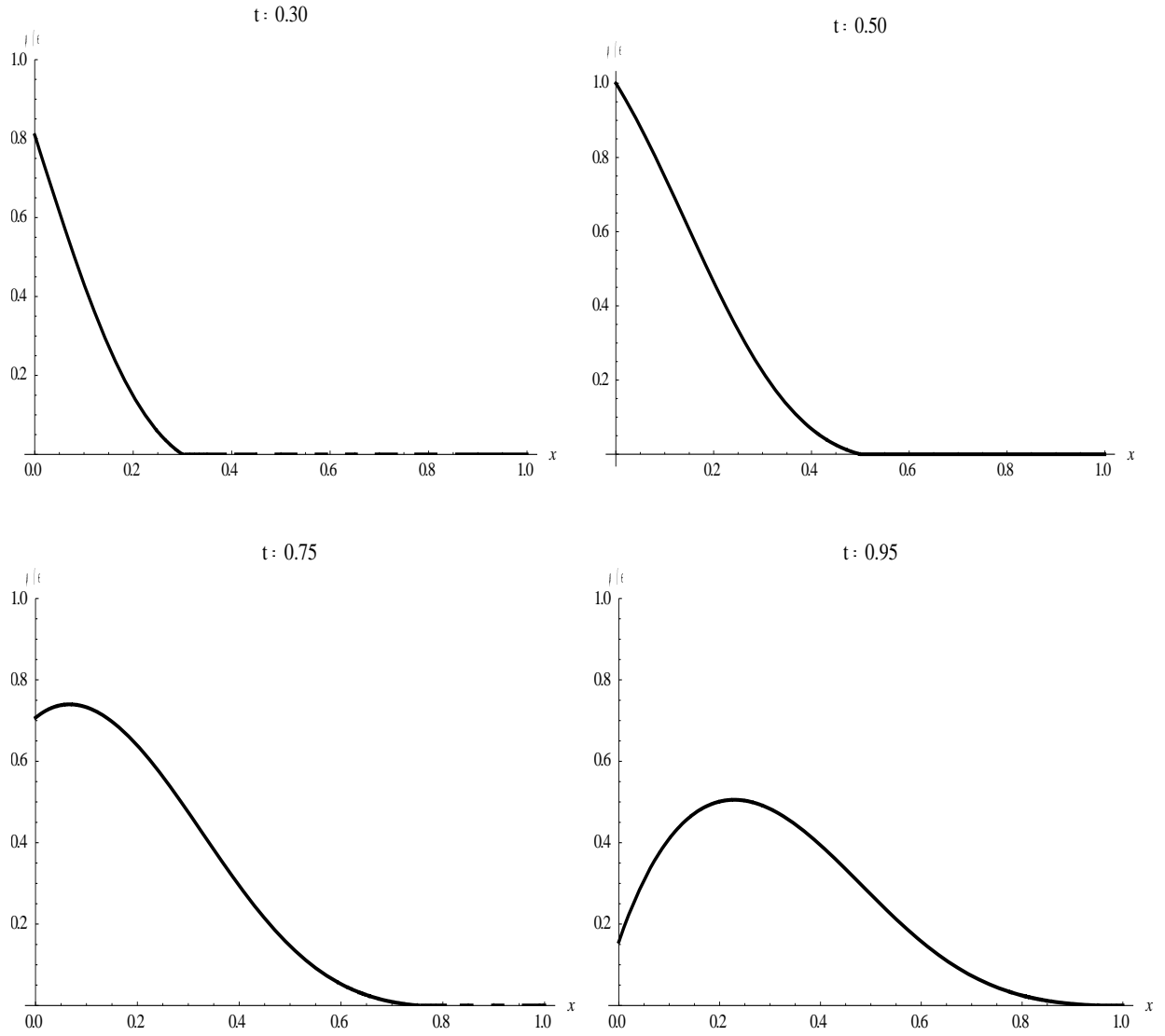
Fig. V: ρ/ε versus x for Zel'dovich law for $\alpha = -0.5$, $\gamma^* = 5.0$ and $\varepsilon = 0.25$.
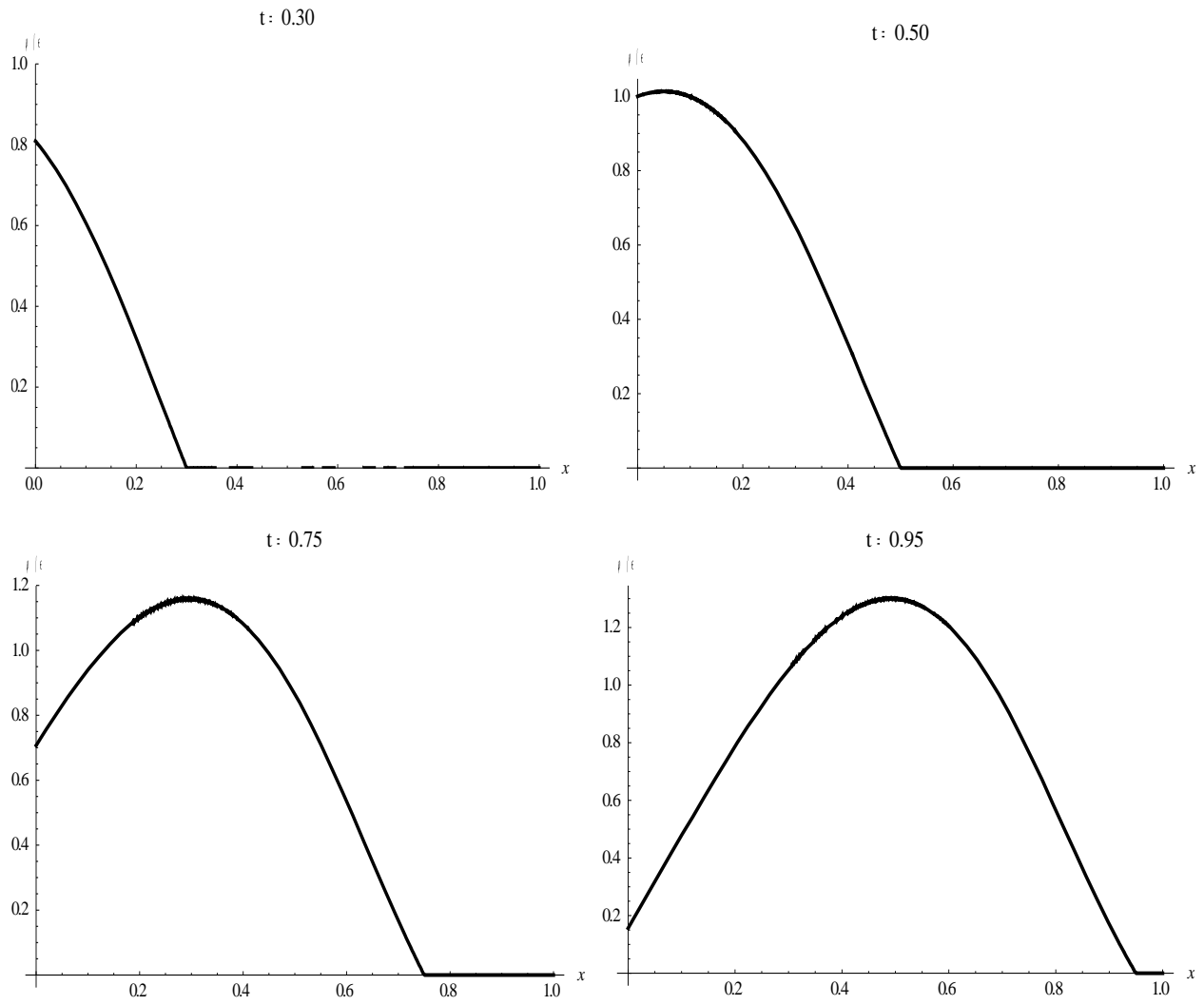
Fig. VI: ρ/ε versus x for Zel'dovich law for $\alpha = 0.0$, $\gamma^* = 5.0$ and $\varepsilon = 0.25$.

t : 0.30

t : 0.50

t : 0.75

t : 0.95
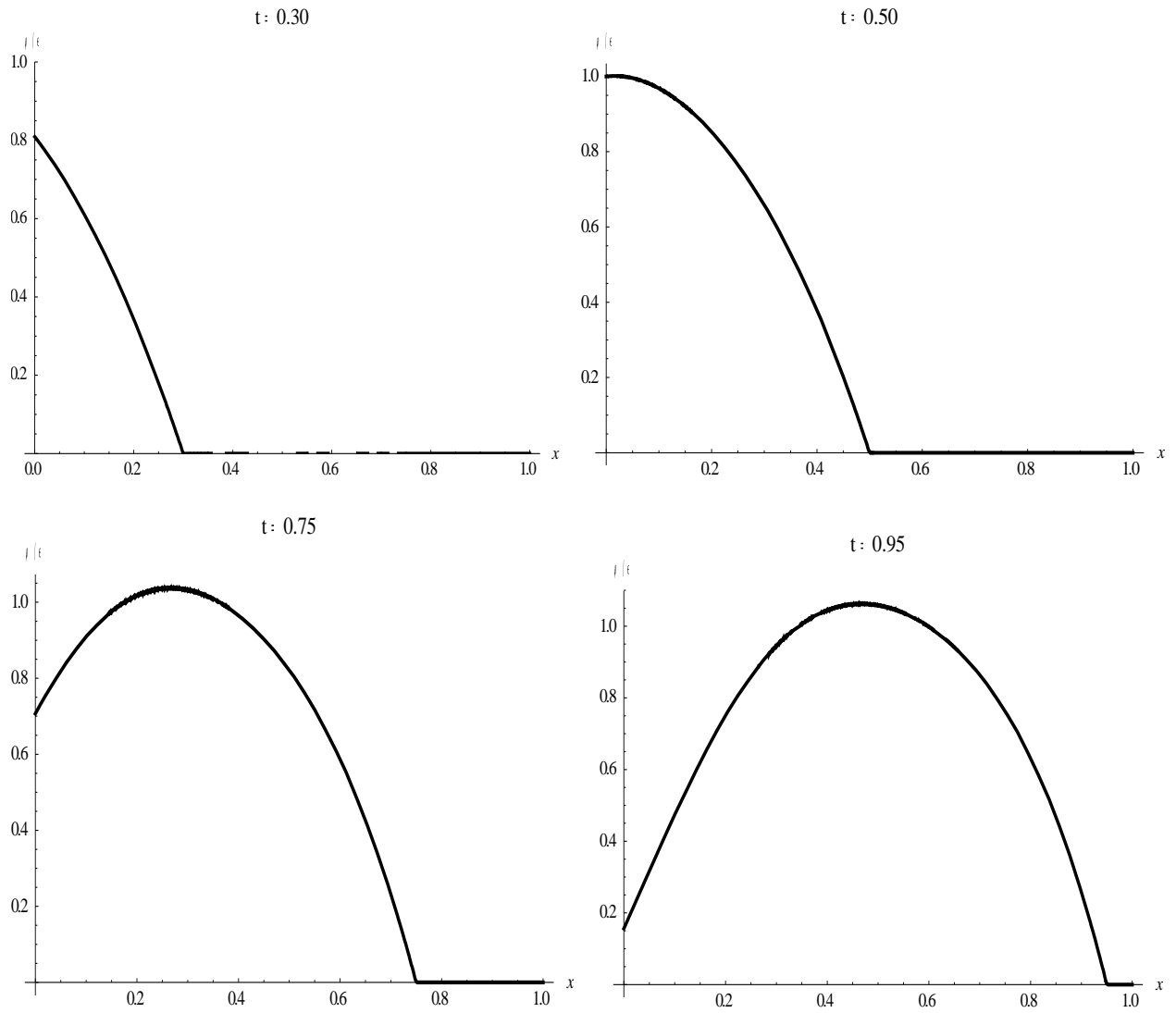
Fig. VII: ρ/ε versus x for Zel'dovich law for $\alpha = 0.5$, $\gamma^* = 5.0$ and $\varepsilon = 0.25$.
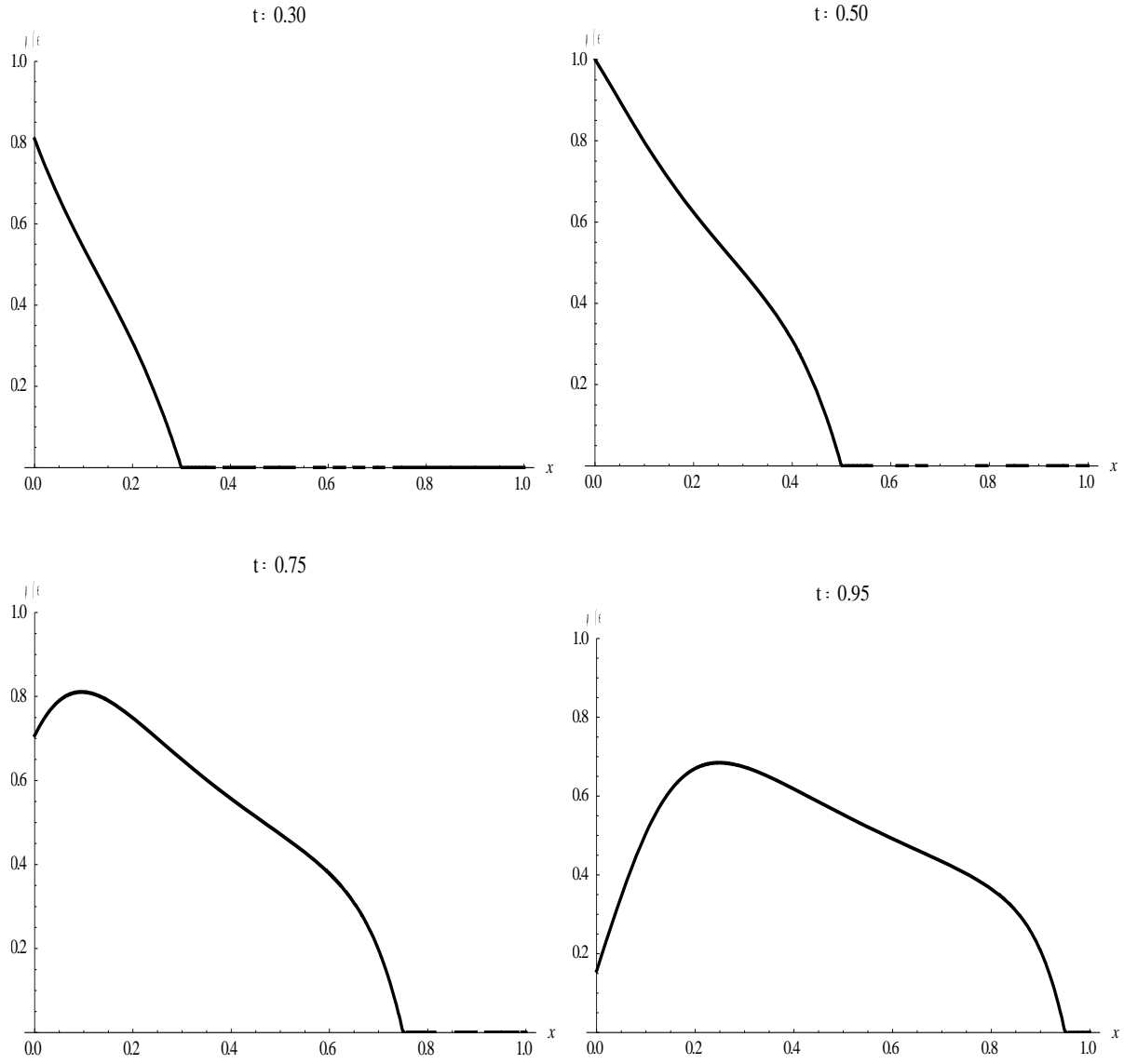
Fig. VIII: ρ/ε versus x for Zel'dovich law for $\alpha = 0.5$, $\gamma^* = 5.0$ and $\varepsilon = 1.0$.

In Fig. V, attenuation is observed. In all the frames of figure V, it is clear that the peak value of ρ is less than 0.5. Since the coefficient of ρ_t is strictly negative for either $\rho > 0.5$ or $\rho < 0.5$ whenever $\alpha = -0.5$, attenuation is expected. Unlike in figure V, the profile ρ/ε versus x undergoes amplification in figure VI when $\alpha = 0.0$ and $\varepsilon = 0.25$; in this case, the coefficient of ρ_t is negative for $\rho > 2/3$ (i.e. attenuation) and positive for $\rho < 2/3$ (i.e. amplification). The amplification is expected as the peak value of ρ is still less than 2/3 even in the fourth frame of Fig. VI. For a positive value of α, the sign of the coefficient of ρ_t is bounded by $(2 - 3\alpha)/3$. For $\rho > (2 - 3\alpha)/3$, the coefficient is strictly negative whereas positive for $\rho < (2 - 3\alpha)/3$. Based on this fact, the profile in figure VII for $\alpha = 0.5$ and $\varepsilon = 0.25$ must suffer attenuation since the peak value of ρ, is greater than 0.167, is 0.25 in the last three frames of Fig. VII. Nonetheless, the profile does not remarkably behave so in the graph. To obtain a clear picture, α is held constant at 0.5 and the amplitude of the input impulse is increased to 1, i.e. $\varepsilon = 1.0$. The plot of evolution of ρ/ε versus x over time shows that the negative growth becomes prominent for $\varepsilon = 1.0$ as shown in Fig. VIII. This confirms that ρ diminishes for $\rho > (2 - 3\alpha)/3$ as the peak value of ρ is greater than 0.167 in all frames of figure VIII.

3.3 Newmann Law

Applying the integral approach, the TWS for Newmann law (for a special case of $\kappa = 0$) given by

$$f = \pm \frac{1}{\sqrt{1 - AExp\left[\dfrac{2\gamma\xi\upsilon}{\beta(\upsilon^2 - c_\infty^2)}\right]}} \ ,$$

where A is a constant. Again, the above TWS has the same form as in literature [8] for a special case.

The sequences of the figures IX – XI depict the evolution of normalized relative density profiles ρ/ε versus x in the interval $x \in (0, 1)$ for Newmann law and correspond to $\alpha < 0$, $\alpha = 0$ and $\alpha > 0$, respectively.
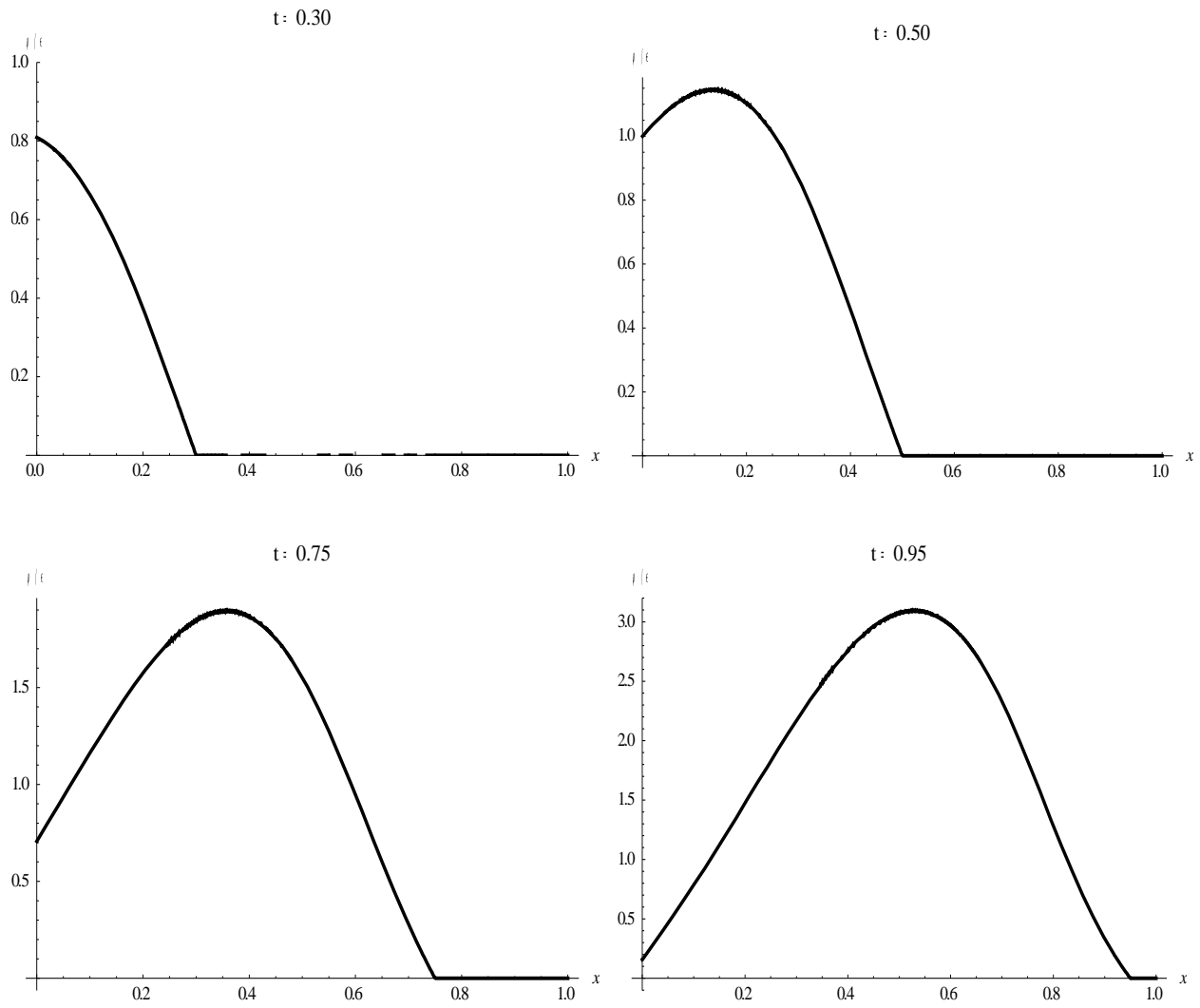
Fig. IX: ρ/ε versus x for Newmann law for $\alpha = -0.5$, $\gamma^* = 5.0$ and $\varepsilon = 0.25$.
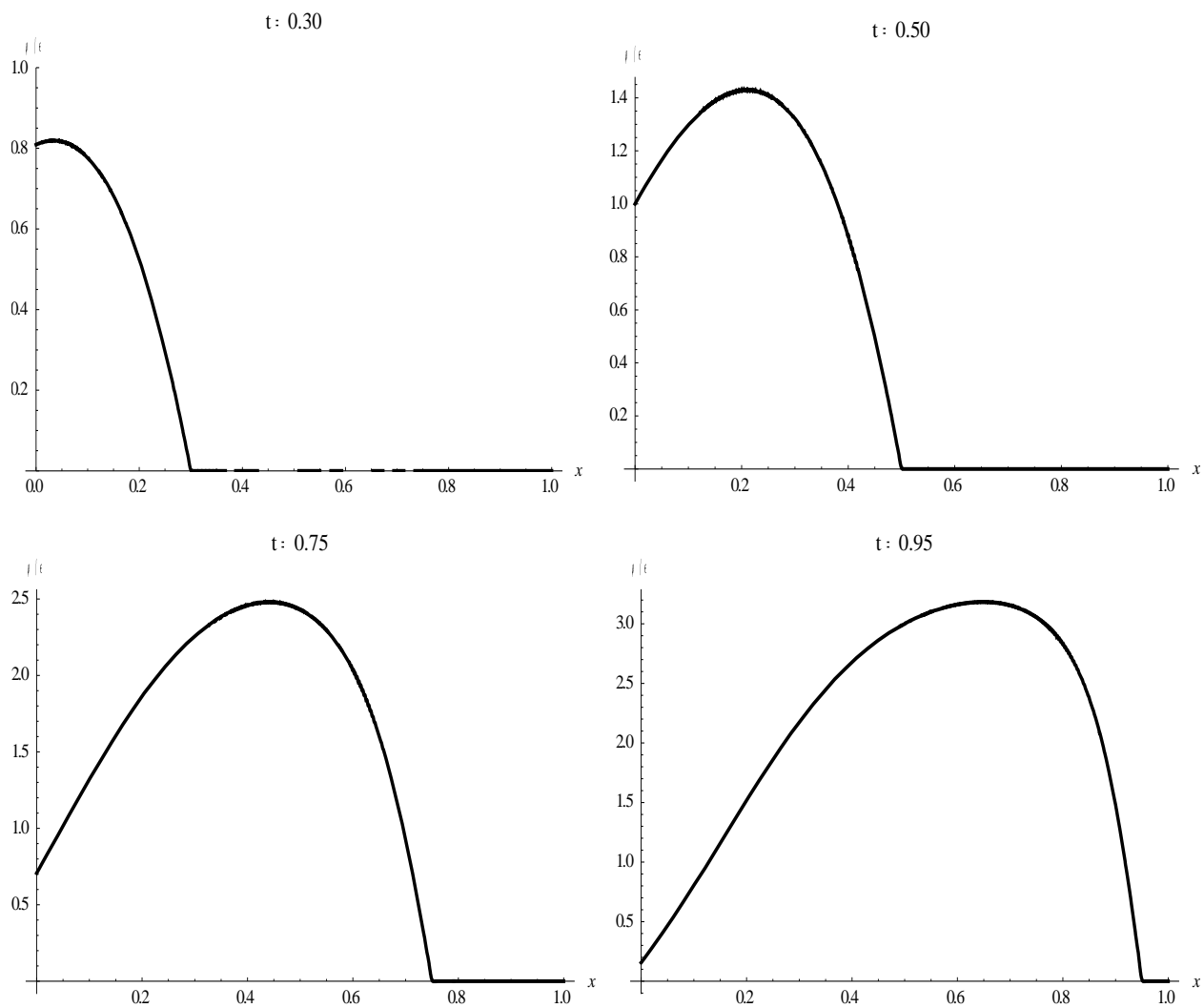
t : 0.30

t : 0.50

t : 0.75

t : 0.95

Fig. X: ρ/ε versus x for Newmann law for $\alpha = 0.0$, $\gamma^* = 5.0$ and $\varepsilon = 0.25$.
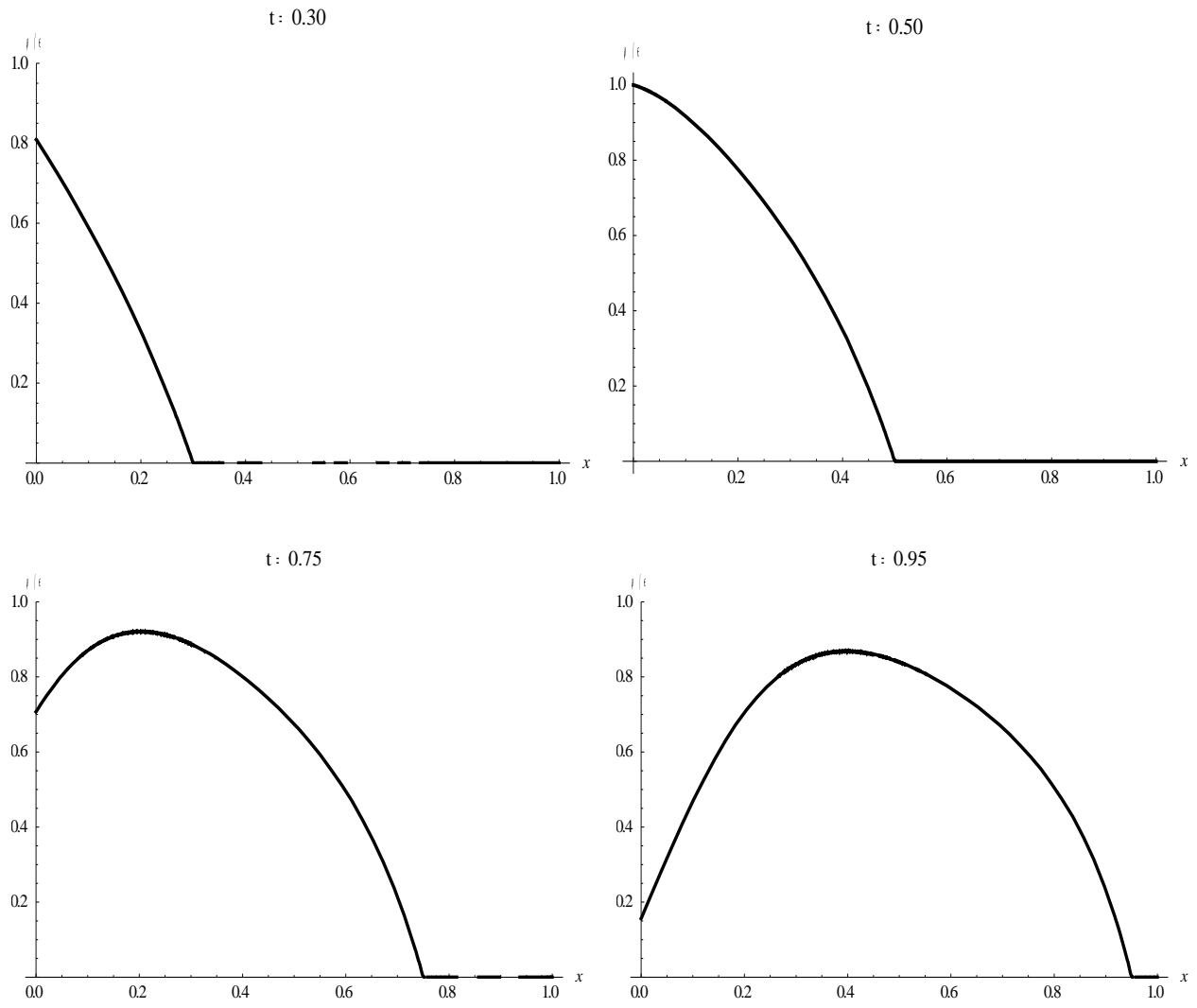
Fig. XI: ρ/ε versus x for Newmann law for $\alpha = 0.0$, $\gamma^* = 5.0$ and $\varepsilon = 0.25$.
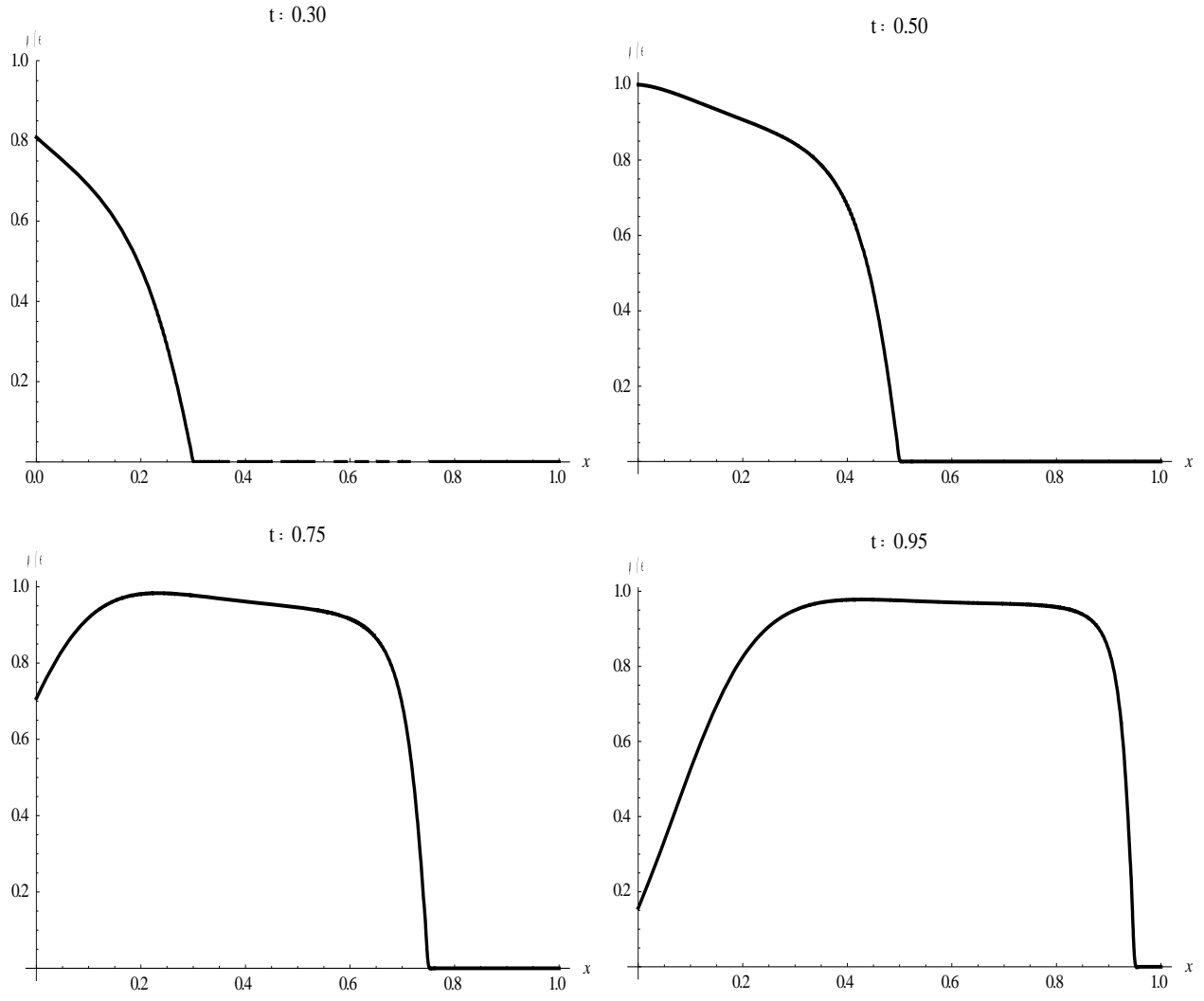
Fig. XII: ρ/ε versus x for Newmann law for $\alpha = 0.0$, $\gamma^* = 5.0$ and $\varepsilon = 1.0$.

For Newmann law, the coefficient of ρ_t is strictly negative for $(\rho + \alpha)^2 > 1/3$, the analysis is constrained for different values of α within the interval (-1, 1). As shown in figure IX, the relative density profile over time amplifies because $(\rho + \alpha)$ becomes $(\rho - 0.5)$ whose square turned out to be less than 1/3. Even the peak value of ρ is 0.75 at t = 0.95 for α = - 0.5, γ^* = 5.0 and ε = 0.25. Therefore, amplification is expected in Fig. IX. However, it should be noted that as the value of α is gradually decreased from - 0.5, the square term increases and at a certain value of α, it exceeds 1/3. By slightly altering the values of α towards -1 while keeping other parameters constants, it is found that the lower bound on α is $-$ 0.70 for γ^* = 5.0 and ε = 0.25. For $- 1 < \alpha < - 0.70$, the attenuation is witnessed as anticipated. Now, the value of α is increased towards 1. Fig. X clearly displays that the profile suffers positive growth over time for $\alpha = 0$. The peak value of ρ exceeds 1/3 by t = 0.5 and the square of its peak value exceeds 1/3 by t = 0.75. This surprising growth is not predicted by the coefficient of ρ_t in equation (18a) for Newmann law. In fact, the upper bound on α is spotted to be 0.45, after which attenuation becomes prominent. As depicted in Fig. XI, the relative density profile suffers attenuation for $\alpha = 0.50$, γ^* = 5.0 and $\varepsilon = 0.25$ as normal.

To see if the contradictory negative attenuation observed in Fig. X extends further, ε is altered from 0.25 to 1.0 holding α constant. The time evolution of ρ/ε versus x over time shows that there is not only no indication of amplification but also a slight diminution in the peak value of profile as shown in Fig XII.

3.4 Stefan-Boltzmann Law

Similarly, the implicit TWS for Stefan-Boltzmann law for $\kappa = 0$ is found to be

$$2ArcTan\left[\frac{\rho_s}{f}\right] + \ln\left[\frac{f - \rho_s}{f + \rho_s}\right] = 4\gamma\upsilon\left(\frac{\xi}{\beta(\upsilon^2 - c_\infty^2)} + \text{constant}\right).$$

The sequences of the figures XIII − XVII depict the evolution of normalized relative density profiles ρ/ε versus x in the interval $x \in (0, 1)$ for Stefan-Boltzmann law and correspond to $\alpha < 0$, $\alpha = 0$ and $\alpha > 0$ respectively.
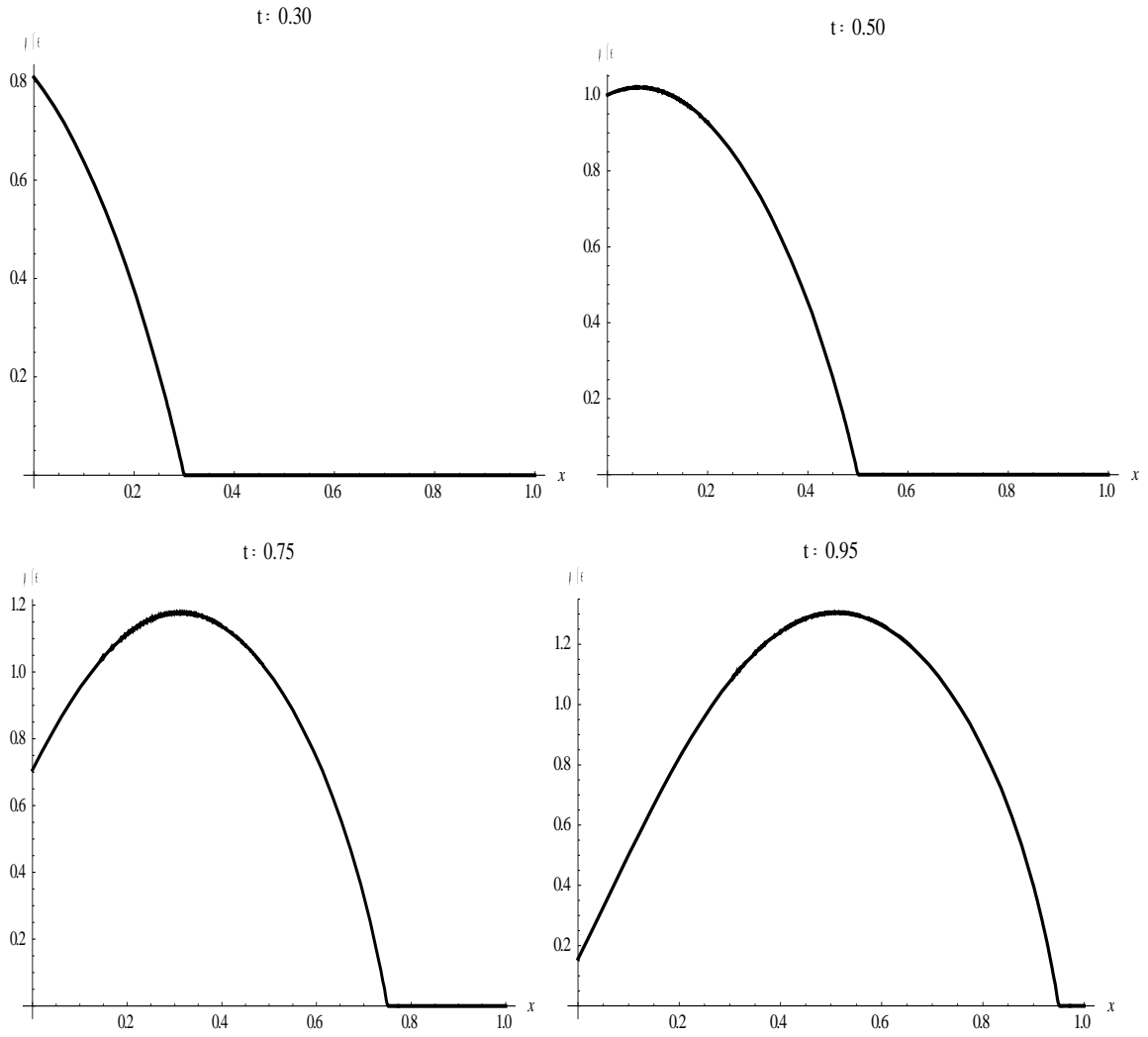
Fig. XIII: ρ/ε versus x for Stefan-Boltzmann law for $\alpha = -0.5$, $\gamma^* = 5.0$ and $\varepsilon = 0.25$.
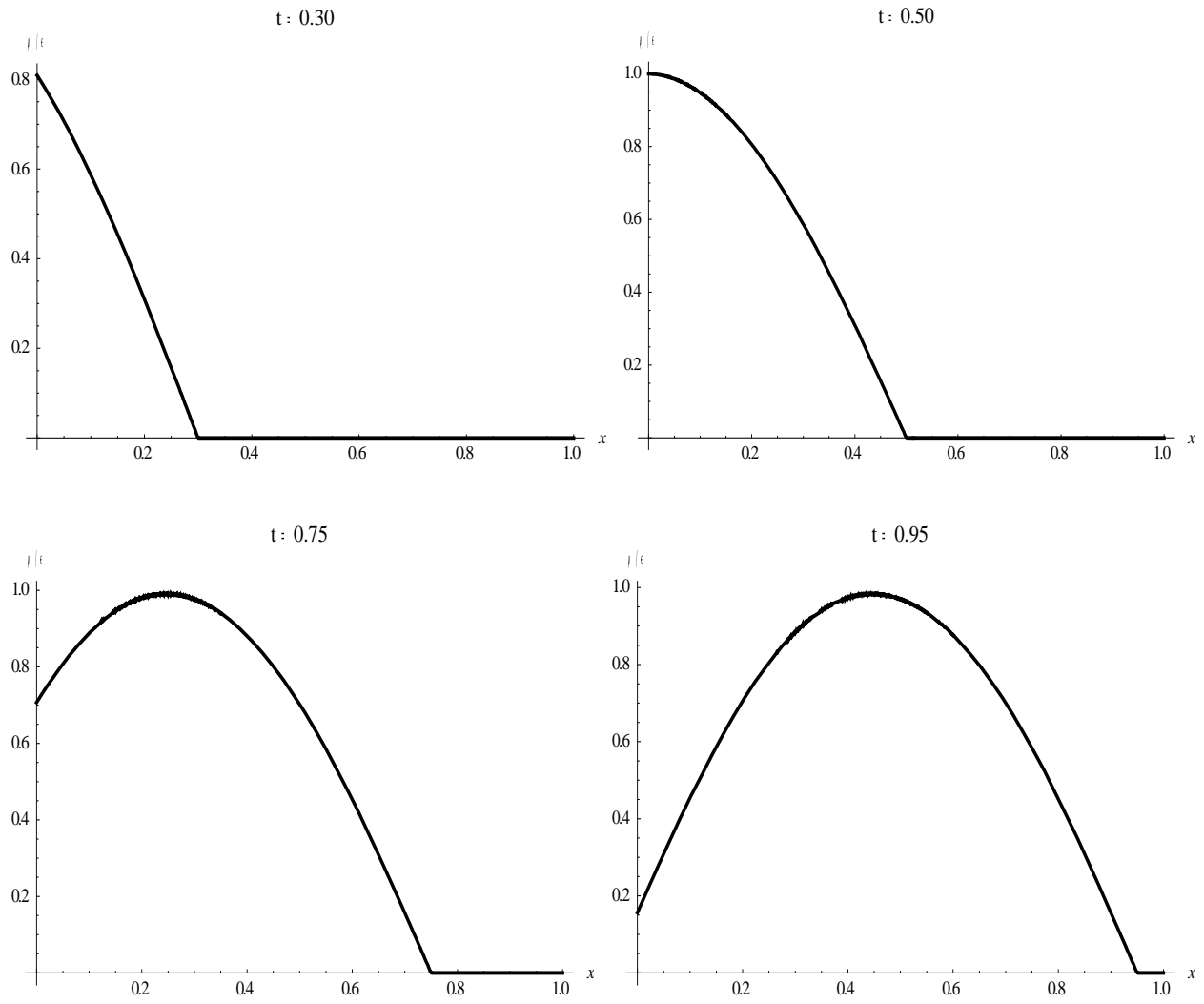
Fig. XIV: ρ/ε versus x for Stefan-Boltzmann law for $\alpha = 0.0$, $\gamma^* = 5.0$ and $\varepsilon = 0.25$.
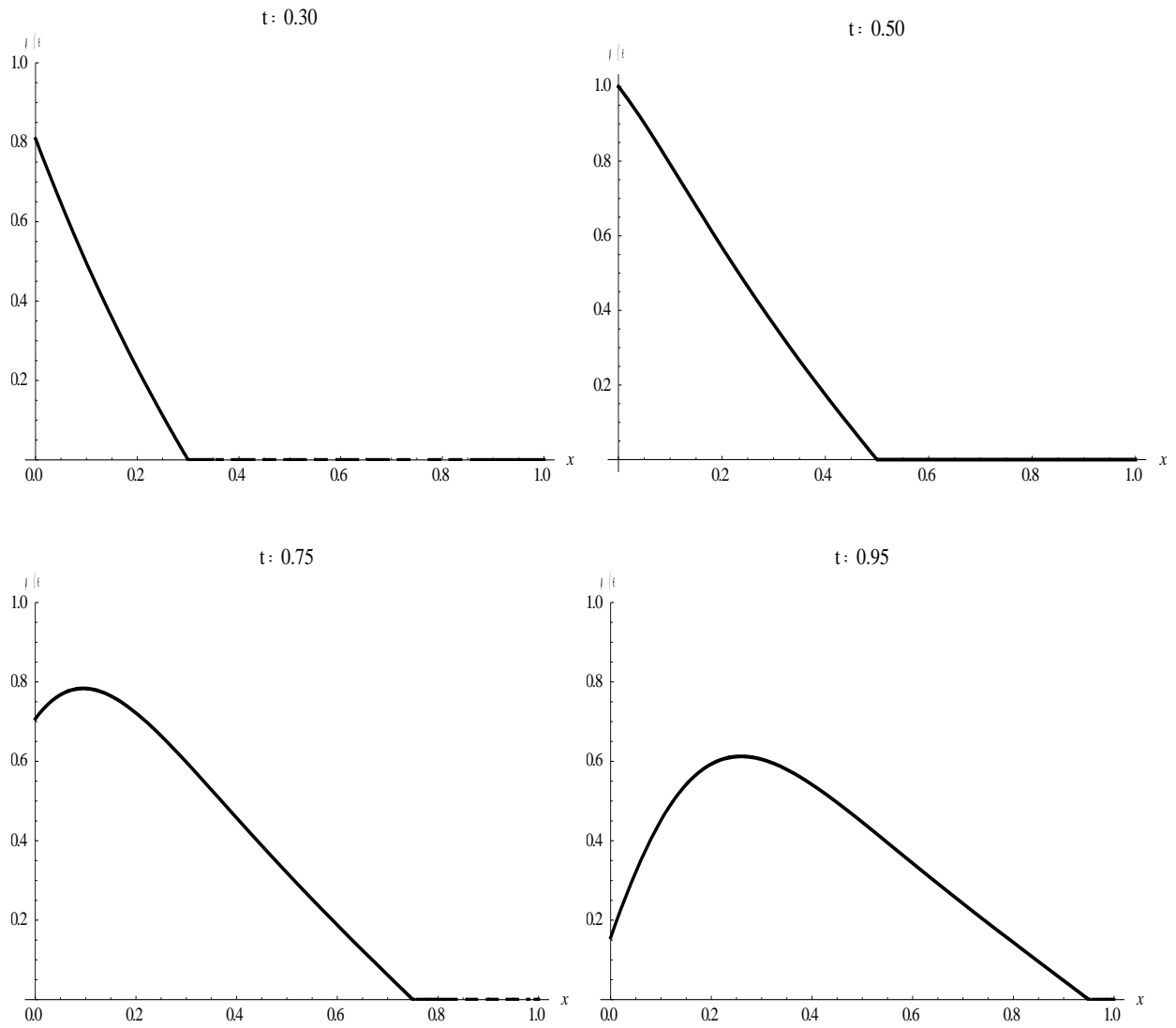
Fig. XV: ρ/ε versus x for Stefan-Boltzmann law for $\alpha = 0.5$, $\gamma^* = 5.0$ and $\varepsilon = 0.25$.
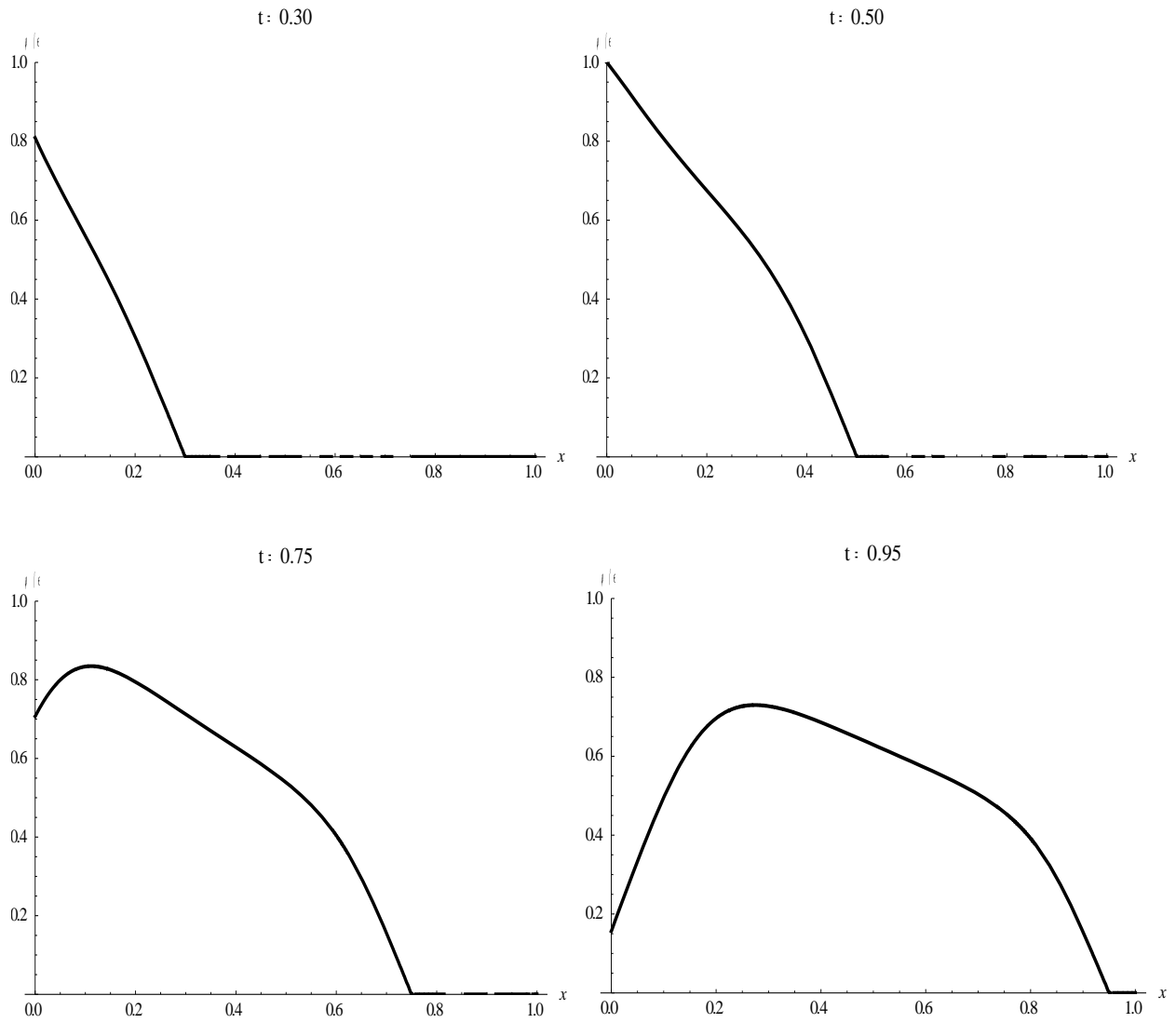
Fig. XVI: ρ/ε versus x for Stefan-Boltzmann law for $\alpha = 0.0$, $\gamma^* = 5.0$ and $\varepsilon = 1.0$.

In figure XIII, which was generated for $\alpha = -0.5$, $\gamma^* = 5.0$ and $\varepsilon = 0.25$, positive growth is observed. This is exactly what one should expect for this case based on the fact that the coefficient of the term ρ_t is strictly positive as long as the value of ρ is less than $-\alpha$. It is also clear from the last frame of Fig. XIII that even the peak value of ρ, which is 0.3, is less than 0.5. As α becomes more negative, amplification dominates. Upon slightly changing the value of α towards 0, we found that the positive growth of the profile completely diminishes at $\alpha = -0.3$ and finally, the profile represent the general hyperbolic wave with no damping. When $\alpha = 0.0$, $\gamma^* = 5.0$ and $\varepsilon = 0.25$, the profile still shows no effect of damping as shown in Fig. XIV. This result seems to contradict the prediction that the damping coefficient for this particular case turns out to be strictly negative (and hence negative growth). However, when the profile of relative density versus space is plotted for $\alpha = 0.5$, $\gamma^* = 5.0$ and $\varepsilon = 0.25$, attenuation is detected as shown in Fig. XV, which approves the anticipated effect of damping coefficient in equation (18a). To see if the contradictory negative attenuation observed in Fig. XIV extends further, ε was converted from 0.25 to 1 with α held constant. The time evolution of ρ/ε versus x over time shows a strong negative growth of profile as shown in Fig XVI.

Conclusion

To sum up, a general equation for a class of diffusion models is successfully formulated. It is shown that implicit TWS can be derived by using the integral equation approach. Moreover, the explicit TWS for Pearl-Verhulst growth law and Newmann law were successfully derived directly from the integral approach. Similarly, the numerical analysis is successfully conducted for the mentioned cases of the general source. Following attenuation analysis and comparison with the literature [1], it is noted that the damping effect becomes pronounced when the strength of the input impulse is amplified and singular surface analysis should be conducted to completely understand the overall impact of the input transient signal.

References

[1] P. M. Jordan. Growth, Decay and bifurcation of shock amplitdues under the type-II flux law. *Proceedings of the Royal Society London A* (2007), **463**, 2783-2798.

[2] J. Philibert. One and a Half century of Diffusion: Fick, Einstein, before and beyond. *Diffusion Fundamentals* 2 (2005), 1.1-1.10.

[3] A. Fick. On liquid diffusion. *Philosophical Magazine (1855)*, **10**, 30–39.

[4] J. Eslick . A Dynamical Study of the Evolution of Pressure Waves Propagating through a Semi-Infinite Region of Homogeneous Gas Combustion Subject to a Time-Harmonic Signal at the Boundary. *University of New Orleans Theses and Dissertations*. *Paper* 1367. 2011.

[5] R. A. Fisher. The wave of advance of advantageous genes. *Annals of Eugenics*. (1937), **7**, 355-369.

[6] A. Kolmogoroff, I. Petrovsky& N. Piscounoff. Étude de l'équations de la diffusion aveccroissance de la quantité de matiére et son application a un probléme biologique. *Bulletin University of Moskow*, *Ser. International Sec. A* **1**, 1-25.

[7] Mark J. Ablowitz & A. Zeppetella. Explicit solutions of Fisher's Equation for a special wave speed. *Bulletin of Mathematical Biology*, **41**, 835-840.

[8] S. Bargmann. Computational modeling of material behavior on different scales based on continuum mechanics, 157-179.

[9] Y. B. Zeldovich, *et. al*. The mathematical theory of combustion and explosions (New York: Consultants Bureau) (1985).

[10] A. C. Newell and J. A. Whitehead. Finite bandwidth, finite amplitude convection. *Journal of Fluid Mechanics (1969)*, **38**, 279–303.

[11] W. I. Newman. Some exact solutions to a non-linear diffusion problem in population genetics and combustion. *Journal of Theoretical Biology (1980), 85*, 325–334.

[12] G. Rosen. Stability of pressure waves in a combustion field. *Am. Rocket Soc. J. (1960), 30*.

[13] J. Stefan. Über die beziehung zwischen der wärmestrahlung und der temperatur. *Sitzungsberichte der mathematisch-naturwissenschaftlichen Classe der kaiserlichen Akademie der Wissenschaften (1879)*, Bd. **79** , 391–428.

[14] L. Boltzmann, Ableitung des stefan'schen gesetzes, betreffend die abhängigkeit derwärmestrahlung von der temperatur aus der electromagnetischen lichttheorie. *Annalen der Physik und Chemie (1884)*, Bd. **22** , 291–294.

[15] C. Cattaneo. Atti del seminario matematico e fisico della universita di modena. *In Atti del Seminario Matematico e Fisico della Universita di Modena (1948)* **3**, 3–21.

[16] A.E. Green and P.M. Naghdi. Thermoelasticity without energy dissipation. *Journal of Elasticity Springer Netherlands* (1993), **31,** 189–208.

[17] D. Aronson and H. Weinberger. Multidimensional nonlinear diffusions arising in population genetics. *Advances in Mathematics (*1978), **30**, 33–76.

[18] W. Malfliet. Solitary wave solutions of nonlinear wave equations. *American Journal of Physics (1992)*, **60**, 650.

[19] J. Zhang. Exact and explicit solitary wave solutions to some nonlinear equations. *International Journal of Theoretical Physics (Aug 1996)*, **35**, 8, 1793 − 1798.

[20] X. Y. Wang. Exact and explicit solutions for the generalized fisher equation. *Physics Letters A (22 August 1988)*, **131**, 4- 5, 277 − 279.

[21] Numerical Solution of Partial Differential Equations. Advanced Numerical Differential Equation Solving in Mathematica. Mathematics and Algorithms. Virtual Book. *Wolfram Mathematica 9 Documentation Center.*

<http://reference.wolfram.com/mathematica/tutorial/NDSolvePDE.html>

APPENDIX A: Mathematica Code for *NDSolve* and *Plot* methods

- NDSolve[$\{D[\rho[t,x],\{t,2\}] == D[\rho[t,x],\{x,2\}] + \gamma^*D[u[t,x],t] * (u[t,x] + \alpha)^{m-1}(m - n * (u[t,x] + \alpha)^{n-m}), u[0,x] == 0, \text{Derivative}[1,0][u][0,x] == 0, u[t,1] == 0, u[t,0] == \epsilon\text{Sin}[\pi t]\}, u, \{t,0,1\}, \{x,0,1\}, \text{Method} \rightarrow \{\text{"MethodOfLines"}, \text{"SpatialDiscretization"} \rightarrow \{\text{"TensorProductGrid"}, \text{MinPoints} \rightarrow 1000, \text{PrecisionGoal} \rightarrow 2\}\}$]

- Plot[Evaluate[$\frac{\text{First}[u[0.95,x]/.\#]}{\epsilon}$], $\{x,0,1\}$, PlotRange $\rightarrow$ All, AxesLabel $\rightarrow$ $\{x, "\rho/\epsilon"\}$, PlotLabel $\rightarrow$ "t = 0.95", PlotStyle $\rightarrow$ {Black, Thickness[0.006]}]

APPROVAL SHEET

This is to certify that Ganesh Tiwari has successfully completed his Senior Honors
Thesis, entitled:

Numerical Analysis of Non-Fickian Diffusion with a General Source

_____ Director of Thesis
Ashok Puri

_____ for the Department
George E Ioup

_____ for the University
Abu Kabir Mostofa Sarwar   Honors Program

April 19, 2013
Date